T10 Inversion from multi-spectral experimental techniques

C. RODIET*, B. REMY*, A. DEGIOVANNI*

* LEMTA, Université de Lorraine et CNRS, Vandoeuvre-lès-Nancy, France.

Email Author1 : christophe.rodiet@univ-lorraine.fr ; or :christophe.rodiet@univ-amu.fr

Email Author 2 : benjamin.remy@univ-lorraine.fr

Email Author 3 : alain.degiovanni@univ-lorraine.fr

Abstract: In this tutorial, a method based on the Ordinary Least Squares method (OLS) for optimizing the wavelength selection used for the multi-spectral temperature measurement of surfaces exhibiting non uniform temperature-depending emissivity is presented. The goal consists in minimizing the standard deviation of the estimated temperature (optimal design experiment). Two methods for wavelengths selection are presented, sequential and global with or without constraints on the spectral range. Then, the estimated temperature results obtained by a model taking into account up to a second-order polynomial global spectral transfer function of the overall system (including the emissivity) and for different number of parameters and wavelengths are compared. The model is based on the fluxes (Planck's law and without fluxes ratio). Different selection criteria are presented. These points are treated from theoretical, numerical and experimental points of view.

Keywords: Multi-spectral, thermometry, pyrometry, temperature measurement, multi-band, optical measurement, emissivity, optimal wavelengths, infrared thermography.

Nomenclature

n	Flux density, W.m^{-2}
C_1	Constant Planck's law,
C_2	Constant Planck's law, m.K
T	Temperature, K or °C
T_{ij}	Temperature calculated from the wavelength filters λ_i , λ_j

Greek symbols

ε	Emissivity
λ	Wavelength, m
χ	Reduced sensitivity

subscripts, superscripts and other symbols

λ	Spectral
m	Mean
i,j,k	Number of filter λ

10.1 Introduction

The thermal characterization of weakly reflective opaque materials at high temperatures often uses optical methods for measuring space and/or time distributions of temperature [1]. It is usually done by infrared cameras, quantum detectors or photomultipliers (in the case of measurements at shorter wavelengths [2]). The difficulty with this type of measurement is the spatial and time variation of the emissivity of the material making it non-uniform over the sample surface, especially at high temperature where significant oxidation phenomena can occur. One solution is to make a measurement by the multi-spectral method [2-7] (an exhaustive state-of-the-art has been made in [7], or lecture 5 presented by Krapez in this METTI-6 School). Even if the idea is interesting, its implementation is tricky because of the difficulty to choose the adapted wavelengths λ_i. Indeed, they must be chosen "close enough" to overcome emissivity variations of the material (and more generally, the global transfer spectral function of the overall system, including the emissivity), but not "too close" to obtain an uncertainty on the measured temperature lowest as possible. Note that in this paper we speak indifferently of emissivity or global transfer function (of the overall system, including the emissivity), because each transfer function taking values in the range [0;1], so their product with the emissivity will also bounded by 0 and 1. After a presentation of the theoretical principle of the multi-spectral method, our model will be validated through numerical simulations and experiments. The facility is presented in Section 5 and the considered typical variations of emissivity (or more generally, global transfer function) shown in Section 4. These simulated variations of emissivity (or global transfer function) versus wavelength will be used to validate our theoretical model for estimating temperature through an inverse technique based on an Ordinary Least Squares method. The cost function (10.2) will be used in order to estimate this temperature by inverse method. Based on the minimization of the standard deviation of the estimated temperature *T*, sequential and global selection methods will be presented to determine the optimal wavelengths to choose for optimizing the temperature measurement.

10.2 The multi-spectral method

The principle of multi-spectral methods which are based on the use of multiple wavelengths to obtain the value of different physical quantities have been presented by Krapez in the lecture 5 of this METTI-6 School. Here, we focus our attention on a method using direct radiative heat fluxes in order to estimate the temperature of an oxidized cast iron sample.
The estimation model used in this tutorial is an unbiased model (called *TNL.Tabc* model) based on the estimation of fluxes (10.1). This model consider a second-order polynomial model for modeling the overall spectral transfer function (including the emissivity) through three unknown parameters *(a,b,c)* to estimate. In (10.2), $n_i^{\exp}$ represents the flux measured at the experimental wavelength λ_i.

$$n_i\left(T,a,b,c\right)=\left(a+b\lambda_i+c\lambda_i^2\right)\frac{C_1\lambda_i^{-5}}{\exp\left(\dfrac{C_2}{\lambda_i T}\right)-1} \qquad \forall i\in[\![1;N_f]\!] \qquad (10.1)$$

The objective is to find the values of *(T,a,b,c)* that minimize the following cost function:

$$J\left(T,a,b,c\right)=\sum_{i=1}^{N_f}\left(n_i^{\exp}-n_i(T,a,b,c)\right)^2=\left(n_1^{\exp}-n_1(T,a,b,c)\right)^2+.....+\left(n_4^{\exp}-n_4(T,a,b,c)\right)^2 \qquad (10.2)$$

10.3 Selection of the optimal wavelengths for minimum error on the estimated temperature

In this section, criteria allowing us to define the methodology to follow to perform optimal measurements without amplifying the uncertainties will be first established. Then, a method to determine sequentially the best wavelengths will be presented. Even if this method is not optimal, it has an educational interest in showing what happens when the numbers of wavelengths is increasing. To finish, the results of a global optimization (with and without constraints) which gives the "optimal global wavelengths" will be shown. Even if the methods can be applied for any spectral emissivity variation, in order to simplify the interpretation of the results, a unitary emissivity (or global spectral transfer function) will be assumed for the simulation of the "experimental" fluxes used both for the sequential and global methods (cf.section 3). Finally, note that each theoretical optimal wavelength represents experimentally the central wavelength of the narrow filter which will be used with the infrared camera.

10.3.1 Determination of the methodology of the measurement

First, for mono-spectral measurements we will work on the increasing part of the Planck's curve because the reduced sensitivities of flux to the temperature χ_T and to the wavelength χ_λ are greater at short wavelengths (10.3). Secondly, for bi-spectral measurements, we will try to have a flux ratio as large as possible to minimize the measurement uncertainty on the flux (10.4) (assuming that $e_{n_{\lambda_i}} \approx e_{n_{\lambda_j}}$) [5]. In addition, our filters have to be chosen distant enough $\Delta\lambda$ (10.5) to avoid amplification of measurement uncertainties but also close enough to minimize measurement uncertainty due spectral emissivity (or more generally spectral global transfer function including emissivity) variation. However, it can be shown that at very short wavelengths (UV), the relation (10.5) can be linearized and therefore it becomes possible to choose a constant distance between two successive wavelengths. Furthermore, note that the relative uncertainty on the temperature e_T / T [5] is increasing with temperature (10.6). Even if the relations (10.4) and (10.5) have been obtained by differentiating a flux ratio [5] (classical bi-chromatic method, based on the Wien's approximation), they are also valid for the propose method based on (10.1) with *b=c=0*. Finally, note that the relations (10.3) and (10.6) are obtained by differentiating (10.1) under Wien's approximation and with *b=c=0*.

$$\chi_T = \frac{1}{n_\lambda(T)}\frac{dn_\lambda(T)}{dT} \simeq \frac{C_2}{\lambda T^2} \qquad ; \qquad \chi_\lambda = \frac{1}{n_\lambda(T)}\frac{dn_\lambda(T)}{d\lambda} \simeq \left(\frac{C_2}{\lambda T} - 5\right)\frac{1}{\lambda} \tag{10.3}$$

$$\frac{e_{n_{\lambda_i}}}{n_{\lambda_i}} + \frac{e_{n_{\lambda_j}}}{n_{\lambda_j}} = \frac{e_{n_{\lambda_i}}}{n_{\lambda_i}}\left(1 + \frac{n_{\lambda_i}}{n_{\lambda_j}}\frac{e_{n_{\lambda j}}}{e_{n_{\lambda_i}}}\right) \simeq \frac{e_{n_{\lambda_i}}}{n_{\lambda_i}} \qquad \left(\forall (n_{\lambda_i}, n_{\lambda_j}) / \frac{n_{\lambda_i}}{n_{\lambda_j}} << 1\right) \tag{10.4}$$

$$\Delta\lambda = \left|\lambda_j - \lambda_i\right| > \left.\frac{T\lambda_j^{\,2}}{C_2}\right|_{\lambda_i<\lambda_j} \tag{10.5}$$

$$\frac{e_T}{T} = \frac{\lambda T}{C_2}\frac{e_{\varepsilon_{\lambda,T}}}{\varepsilon_{\lambda,T}} \tag{10.6}$$

10.3.2 Determination of best sequential wavelengths

The criteria previously established can allow us to set up a methodology for wavelengths selection. Nevertheless, as they are given in term of inequalities, we are not able to know if the wavelengths choice

is optimal or not. As the method used for temperature estimation is based on the minimization of a functional through an Ordinary Least Squares method (OLS), the idea we propose in this work is to select optimal wavelengths by minimizing the standard deviation of the estimated temperature. In the OLS method, the statistical properties of the parameters (10.2) are given by the variance-covariance matrix, from which the standard deviations σ_{β_i} of estimated parameters and particularly of the temperature σ_T can be determined. The model (10.1) being non-linear, we will use the approximate expression of the variance-covariance matrix of the Ordinary Least Squares method, which is given for a parameter vector $\boldsymbol{\beta} = (T, a, b, c)$, under assumptions of an additive noise, non-correlated, identically distributed (zero mean and constant variance), by:

$$\mathrm{cov}(\boldsymbol{\beta}) = \begin{bmatrix} \sigma_T^2 & \mathrm{cov}(T,a) & \mathrm{cov}(T,b) & \mathrm{cov}(T,c) \\ \mathrm{cov}(T,a) & \sigma_a^2 & \mathrm{cov}(a,b) & \mathrm{cov}(a,c) \\ \mathrm{cov}(T,b) & \mathrm{cov}(a,b) & \sigma_b^2 & \mathrm{cov}(b,c) \\ \mathrm{cov}(T,c) & \mathrm{cov}(a,c) & \mathrm{cov}(b,c) & \sigma_c^2 \end{bmatrix} = \left(X^t X\right)^{-1} \sigma_{noise}^2 \quad ; \quad X = \frac{\partial n_i}{\partial \beta_j} = \begin{bmatrix} \frac{\partial n_1}{\partial T} & \frac{\partial n_1}{\partial a} & \frac{\partial n_1}{\partial b} & \frac{\partial n_1}{\partial c} \\ \vdots & \vdots & \vdots & \vdots \\ \frac{\partial n_N}{\partial T} & \frac{\partial n_N}{\partial a} & \frac{\partial n_N}{\partial b} & \frac{\partial n_N}{\partial c} \end{bmatrix} \quad (10.7)$$

The sequential method consists in choosing the first optimal wavelength (λ_{opt1}) (corresponding experimentally to the central wavelength of the narrow filter which will be used with the infrared camera) minimizing the standard deviation of the temperature, assuming that we perform only a mono-spectral measurement (thus with the only one unknown parameter *T*) (cf. Figures 1 and 2). Note that this value does not correspond to the maximum of the Planck's curve. It can be shown that $\lambda_{opt1} T = C_2 / 6 \approx 2400\,\mu m.K$, to be compared with the Wien's expression $\lambda_{\max} T \approx 2898\,\mu m.K$.

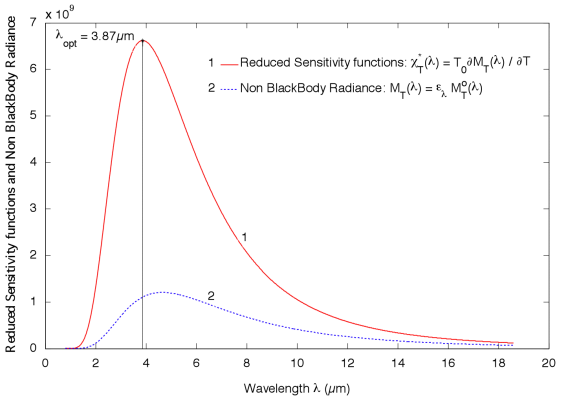

Figure 1. Reduced Sensitivity curves for unitary emissivity with $n_T(\lambda)$ given by (1) and for T_0 = 623K.

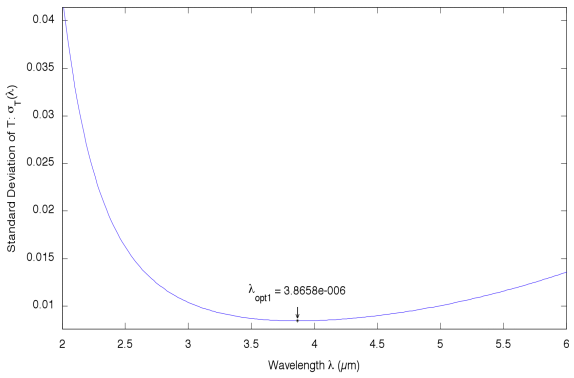

Figure 2. Standard deviation of T for unitary emissivity with σ_T given by (9) and β=623 (just one wavelength and the parameter T).

The value is slightly shifted to the left and appears as a compromise solution between a large sensitivity and a good signal over noise ratio. This result shows the interest of the Ordinary Least Squares method allowing us to define an optimal wavelength for the temperature measurement, contrary to the expression (10.6) that only takes into account the sensitivity aspect and gives for optimal wavelength $\lambda = 0$ because the relative uncertainty on the temperature is null for this value. Figure 2 shows that there is a unique wavelength ($\lambda_{opt1} \approx 3.87\mu m$) that minimizes the standard deviation $\sigma_T(\lambda)$ (for the mono-spectral measurements). The increasing of the standard deviation when the wavelength is decreasing for $\lambda < \lambda_{opt1}$

can be explained by the fact that the signal over noise ratio is decreasing for $\lambda \to 0$. The increasing of the standard deviation for $\lambda > \lambda_{opt1}$ is due to the fact that the sensitivities of flux to the temperature $n_\lambda \cdot \chi_T$ (10.3) are decreasing with the wavelength (Figure 1). Indeed, for a mono-spectral measurement $\sigma_T(\lambda) = \left(n_\lambda \cdot \chi_T\right)^{-1}$ which is similar to the relative uncertainty on the temperature e_T / T (10.6).

Then, in order to choose the value of the second filter, λ_1 is fixed to $\lambda_{opt1} \approx 3.87 \mu m$, and we seek the shortest wavelength ($\lambda_{opt21} \approx 2.64 \mu m$ here) that minimizes the local standard deviation of temperature in the model *TNL.Ta* (cf. Figure 3). The notation (cf. section 4 for more details) *TNL.Ta* means that in (10.1) and (10.2) only the parameters *T* and *a* are considered (i.e. *b=c=0*). λ_{opt21} has been chosen instead of λ_{opt22} because λ_{opt22} is not in the spectral range of the detector and allows us to reduce the working spectral range. Furthermore, note that at $\lambda_2 = \lambda_{opt1} \approx 3.87 \mu m$ there is a vertical asymptote ($\sigma_T \to \infty$). This can be explained by the fact that the numeric system to solve is ill conditioned and leads to infinite uncertainties. There are two unknowns (*T* and *a*) but only one equation, For $\lambda_2 < \lambda_{opt21}$ and $\lambda_2 > \lambda_{opt22}$ the standard deviation $\sigma_T(\lambda_2)$ is increasing because the signal over noise ratio and the sensitivity to the temperature are decreasing, and for $\lambda_{opt21} < \lambda_2 < \lambda_{opt22}$, $\sigma_T(\lambda_2)$ is increasing because the criteria (10.5) is less and less respected.

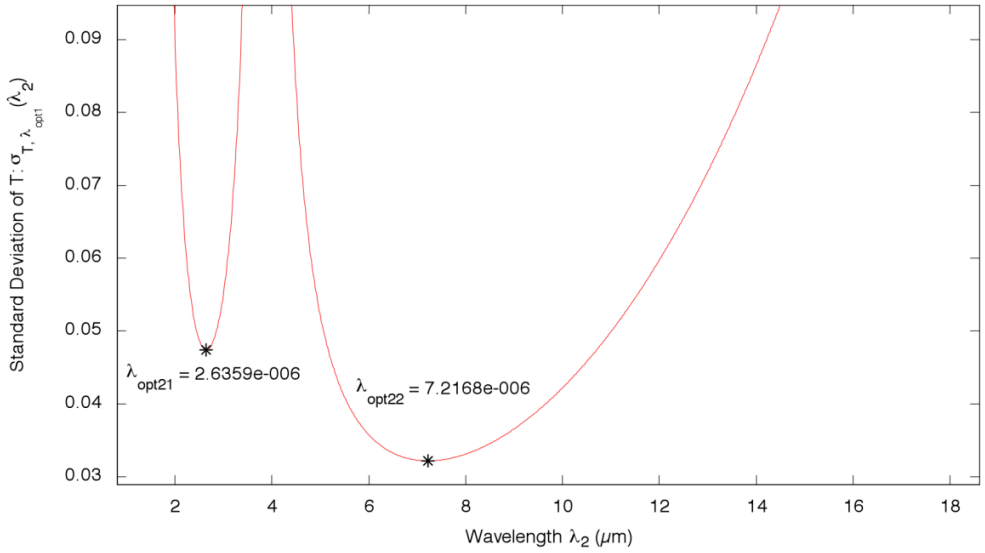

Figure 3. Standard deviation of T for unitary emissivity with $\lambda_1=\lambda_{opt1}$ fixed and λ_2 free ; σ_T given by (9) and β=(623,1) (just one wavelength: λ_2, and two parameters: T and a): Model (T,a).

This procedure is followed for obtaining the fourth wavelength (λ_{opt41}) which minimizes the standard deviation of the temperature in the model (*T,a,b,c)*, with $\left(\lambda_{opt1}, \lambda_{opt21}, \lambda_{opt31}\right)$ fixed. With this process, we finally obtain as set of wavelengths: $\mathbf{l}_{opt\_seq} = \left\{1.67\ ;\ 2.05;\ 2.64\ ;\ 3.87\right\} \mu m$ and $\sigma_T \approx 4\ K$.

Because of experimental constraints (availability of filters), we have chosen the following wavelengths filters: $\mathbf{l}_{exp} = \left\{2\ ;\ 2.35\ ;\ 2.85\ ;\ 4\right\} \mu m$. With these wavelengths and $\boldsymbol{\beta}_0 = \left(623,1,0,0\right)$, the theoretical standard deviation calculated is for $\beta = \left(T,a,b,c\right)$: $\sigma_T \approx 2.55\ K$

Comparing this value with the previous one ($\sigma_T \approx 4\ K$) obtained for $\lambda_{opt\_seq} = \{1.67\ ;\ 2.05;\ 2.64\ ;\ 3.87\}\mu m$ we can see that the wavelengths values obtained through the sequential process are not optimal, but this method presents the advantage of illustrating that it's important to choose carefully the different wavelengths for multispectral measurements.
The next part presents a global optimization of the wavelengths.

10.3.3 Determination of global optimal wavelengths

The determination of $N_f=4$ optimal wavelengths can be done using a global optimization algorithm such as "Nelder-Mead", "Levenberg-Marquardt" or "Trust-Region"... Choosing as nominal parameters vector $\beta_o = (623\ ;\ 1\ ;\ 0\ ;\ 0)$, for an unconstrained estimation the minimization calculus of the standard deviation gives for $\sigma_{noise} \approx 8.9697.10^4\ W \equiv 7.43.10^{-3}\ \%$ of the Planck's law maximum (equivalent to the value of the experimental noise):

- For $\beta = (T,a,b,c)$, we find: $\lambda_{opt\_global} = \{2.53\ ;\ 4.70\ ;\ 8.87\ ;\ 26.18\}\mu m$ and $\sigma_T \approx 0.07\ K$
- For $\beta = (T,a,b)$, we find: $\lambda_{opt\_global} = \{2.67\ ;\ 5.24\ ;\ 12.57\}\mu m$ and $\sigma_T \approx 0.05\ K$
- For $\beta = (T,a)$, we find: $\lambda_{opt\_global} = \{2.94\ ;\ 7.17\}\mu m$ and $\sigma_T \approx 0.02\ K$

For $\lambda_{opt\_global} = \{2.94\ ;\ 7.17\}\mu m$, the Figure 4 shows that the minimum is unique (two symmetric solutions $\{\lambda_1\ ;\ \lambda_2\} \approx \{2.94\mu m\ ;\ 7.17\mu m\}$), and that these solutions are different but leads to better results than those obtain by sequential method $\{\lambda_{opt1}\ ;\ \lambda_{opt22}\} \approx \{3.87\mu m\ ;\ 7.22\mu m\}$.

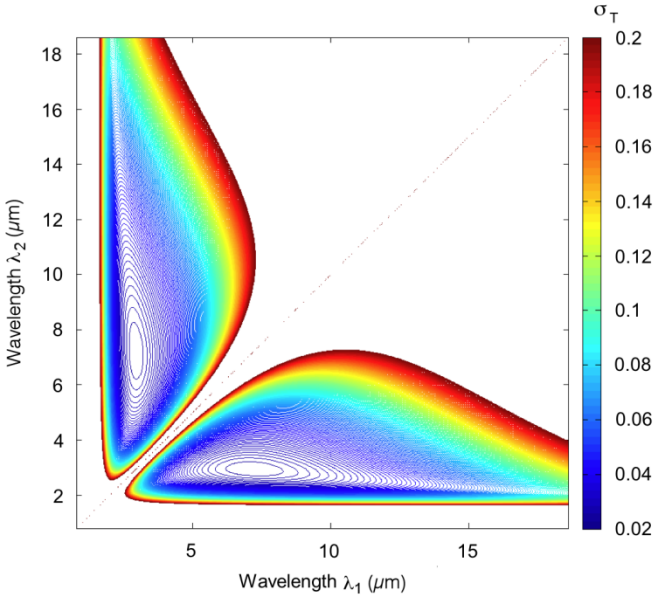

Figure 4. Isovalues of standard deviation of T.

Although this set of values are the best in terms of minimization of the standard deviation, performing measurements at these different wavelengths is difficult in practice because such a detector with a so wide spectral range does not exist. For this reason, we decide to choose our wavelengths only in the spectral range of the detector *[1.5μm; 5.5μm]*. If we perform the global optimization with this constraint, the results obtained are:

- For $\beta = \left(T, a, b, c\right)$, we find: $\lambda_{opt\_cam\_spec\text{-}range} = \left\{2.14\ ;\ 3.39\ ;\ 4.76\ ;\ 5.50\right\}\mu m$ and $\sigma_T \approx 0.32\ K$
- For $\beta = \left(T, a, b\right)$, we find: $\lambda_{opt\_cam\_spec\text{-}range} = \left\{2.43\ ;\ 4.21\ ;\ 5.50\right\}\mu m$ and $\sigma_T \approx 0.09\ K$
- For $\beta = \left(T, a\right)$, we find: $\lambda_{opt\_cam\_spec\text{-}range} = \left\{2.93\ ;\ 5.50\right\}\mu m$ and $\sigma_T \approx 0.03\ K$

But the Wien's approximation being better at short wavelengths, we will force ourselves to choose our wavelengths only in the spectral range corresponding to the increasing part of the Planck curve. In this context, the global estimation with constraint $\lambda \in \left[1.5\mu m\ ;\ 2898\ /\ T\ \mu m\right]$ gives:

- For $\beta = \left(T, a, b, c\right)$, we find: $\lambda_{opt\_\lambda_{max}\_spec\text{-}range} = \left\{2.03\ ;\ 3.11\ ;\ 4.15\ ;\ 4.65\right\}\mu m$ and $\sigma_T \approx 0.52\ K$
- For $\beta = \left(T, a, b\right)$, we find: $\lambda_{opt\_\lambda_{max}\_spec\text{-}range} = \left\{2.32\ ;\ 3.79\ ;\ 4.65\right\}\mu m$ and $\sigma_T \approx 0.14\ K$
- For $\beta = \left(T, a\right)$, we find: $\lambda_{opt\_\lambda_{max}\_spec\text{-}range} = \left\{2.82\ ;\ 4.65\right\}\mu m$ and $\sigma_T \approx 0.03\ K$

Note that in the both global estimation with constraints, the last wavelength is always the upper bound, which means that the best wavelength is probably out of the interval.

10.4 Numerical validation of models for temperature measurement in the infrared wavelength range

To validate the model, thousand noised fluxes are simulated through the Monte-Carlo method (normal noise exhibiting the same level as standard deviation measured on the experimental thermographic images under the same conditions) (cf. Table 2) from four different variations/values of emissivity. We took care that the variations of order 2 and Drude models are significant on the IR spectral range of the study (and in agreement with the experimental behavior of different materials). The tables below show the results for the four filters chosen experimentally. The notation *TNL* means that the temperature is obtained from an "nonlinear least squares" estimation (10.2) using the regularized algorithm of "Levenberg-Marquardt".*TNL.Tabc* (respectively *TNL.Tab*), means that we use (10.2) and the unknown parameters are (*T,a,b,c*) (resp. (*T,a,b*)). For *TNL.Tab,* the three shorter wavelengths will be used.

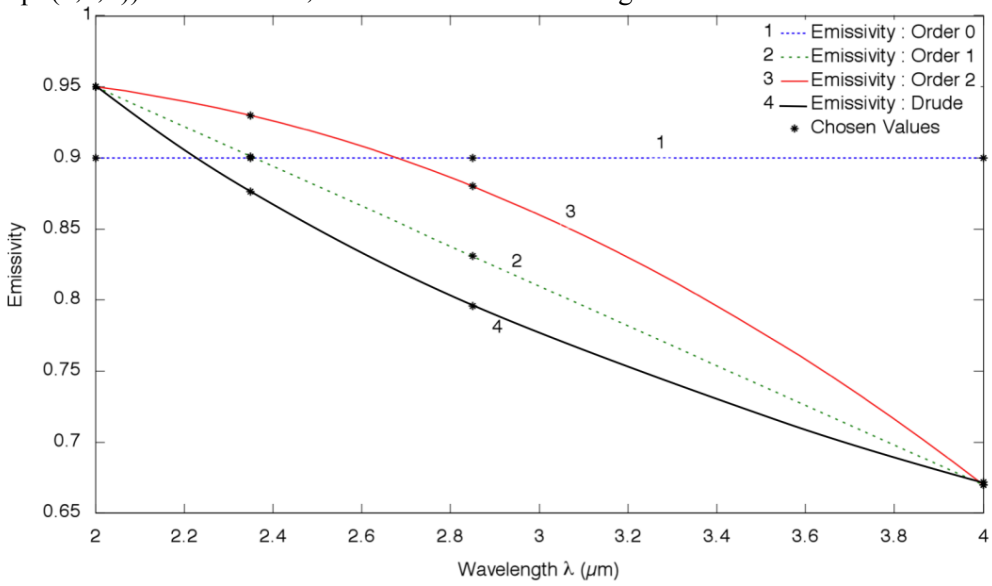

Figure 5. Emissivity variation/values used for numerical validation. The "Chosen Values" are the fixed or calculated values of simulated emissivity at the experimental wavelengths in order

to have significant variations of emissivity compared to the linear variation.

10.4.1 Simulations without noise

lambda [m] = {2e-6; 2.35e-6; 2.85e-6; 4e-6} Texp = 623 K ; Radiance law: Planck							
Noise	Emissivity	Model	T [K]	Absolute Error [K]	Relative Error [%]	Sigma [K]	Sigma [%]
Without	Constant	TNL.Tabc (4bands)	623.00	0.00	0.00	-	-
		TNL.Tab (3bands)	623.00	0.00	0.00	-	-
	Linear	TNL.Tabc (4bands)	623.00	0.00	0.00	-	-
		TNL.Tab (3bands)	623.00	0.00	0.00	-	-
	Order 2	TNL.Tabc (4bands)	623.00	0.00	0.00	-	-
		TNL.Tab (3bands)	608.52	14.48	2.32	-	-
	Drude	TNL.Tabc (4bands)	636.91	13.91	2.23	-	-
		TNL.Tab (3bands)	641.01	18.01	2.89	-	-

Table 1. Simulations for estimating the temperature (without noise).

As models *TNL.Tabc* and *TNL.Tab* do not use Wien's approximation, no bias appears on estimated temperature except for emissivity variation of order 2 for *TNL.Tab,* and Drude for the models *TNL.Tabc* and *TNL.Tab*. The results of this table show that the model *TNL.Tabc* seems to be the better (lowest uncertainties).

10.4.2 Simulations with noise

AVERAGE TEMPERATURE OF 1000 ESTIMATES: lambda [m] = {2e-6; 2.35e-6; 2.85e-6; 4e-6} Texp = 623 K ; Radiance law: Planck ; Noise: constant ; Sigma Noise: 0.00743 % (max of Planck's law)							
Noise	Emissivity	Model	T [K]	Absolute Error [K]	Relative Error [%]	Sigma [K]	Sigma [%]
With	Constant	TNL.Tabc (4bands)	623.02	0.02	0.00	1.13	0.18
		TNL.Tab (3bands)	623.00	0.00	0.00	0.52	0.08
	Linear	TNL.Tabc (4bands)	623.01	0.01	0.00	0.70	0.11
		TNL.Tab (3bands)	623.00	0.00	0.00	0.32	0.05
	Order 2	TNL.Tabc (4bands)	623.02	0.02	0.00	1.05	0.17
		TNL.Tab (3bands)	608.52	14.48	2.32	0.30	0.05
	Drude	TNL.Tabc (4bands)	636.91	13.91	2.23	0.74	0.12
		TNL.Tab (3bands)	641.01	18.01	2.89	0.38	0.06

Table 2. Monte Carlo simulations for estimating the temperature (with noise).

Table 2 shows that it is impossible by the method *TNL.Tabc* to accurately estimate the temperature because the problem seems to be ill-posed. This observation is confirmed by the best results given by *TNL.Tab* in the case of emissivities ranging up to order 2, which shows that it is possible to regularize the problem by reducing the number of parameters. Nevertheless, it is important to note that the standard deviations of the estimations are significant, suggesting that it will be necessary to have lot of points (high spatial resolution allowing a local averaging) or to use larger integration times if we want to increase the measurement accuracy. From these results, we will choose the *TNL.Tabc* model as estimation model for the experiments.

10.5 Experimental results

10.5.1 Description of the experimental bench

The schematic diagram of the facility is shown in Figure 6. An oxidized cast iron sample on which "FT 25" is carved (its surface being varied, so it is for the emissivity) is placed in a tube furnace at a temperature of 623K controlled by a PID with a great stability (no oscillations in temperature recording due to furnace regulation). The temperature of the sample is obtained using a thermocouple placed on its rear face. The spatial radiative flux emitted by the sample is measured through a high sensitive Broad-Band InSb infrared matrix camera working in the spectral range [1.5µm; 5.5µm]. Four monochromatic filters: $\boldsymbol{\lambda}_{exp} = \left\{2\ ;\ 2.35\ ;\ 2.85\ ;\ 4\right\}\mu m$ are mounted in the filters wheel of this camera in order to measure the emitted flux coming from the sample at four different wavelengths. The signal is digitized through a 14 bits Analog/Digital card. Each pixel is associated to a Digital Level (DL) corresponding to the spectral radiance of a surface area of the sample. The camera has previously been calibrated in the temperature range [573K-673K] using a 4"x4" extended area blackbody.

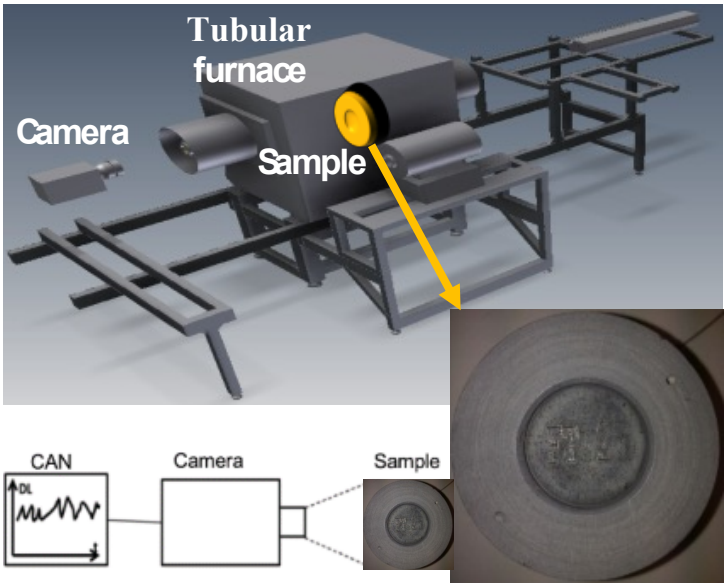

Figure 6. Facility for IR measurements.

10.5.2 Measurement methodology, data processing and results

Using a tubular furnace, the sample is heated at three different temperatures levels {T1 = 573K, T2 = 623K, T3 = 673K}. For each temperature, a recording of 1000 images for each filter is performed. Before each acquisition, great care is taken to check whether thermal equilibrium is reached. To get free of the reflection through the non-blackbody sample that is not negligible at this level of temperature due to presence of the hot furnace walls in this vicinity, we use the average image made with 4 filters at 573K and 673K to correct the existing offset between our measurements at these two temperatures and the flux that a blackbody at these same temperatures would emit. Calling $M_{l_i}^{\exp}\left(T_j\right)$ the experimental heat flux measured for each pixel at the wavelengths λ_i and at the temperature T_j, and K_i a variable to correct the offset between the measured flux and the blackbody flux, we have a set of 8 equations with 8 unknowns (the four couples $\left(\varepsilon_i\ ;\ K_i\right)$) to solve. The system is as follows:

$$M_{\lambda_i}^{\exp}\left(T_j\right) = \varepsilon_i M_{\lambda_i}^{o} + K_i \quad ,\forall i \in [\![1\,;4]\!] \;\; and \;\; \forall j \in \{1\,;3\}$$

$$\Leftrightarrow \begin{cases} M_{\lambda_1}^{\exp}\left(T_1\right) = \varepsilon_1 M_{\lambda_1}^{o} + K_1 \\ \vdots \\ M_{\lambda_4}^{\exp}\left(T_1\right) = \varepsilon_4 M_{\lambda_4}^{o} + K_4 \\ M_{\lambda_1}^{\exp}\left(T_3\right) = \varepsilon_1 M_{\lambda_1}^{o} + K_1 \\ \vdots \\ M_{\lambda_4}^{\exp}\left(T_3\right) = \varepsilon_4 M_{\lambda_4}^{o} + K_4 \end{cases} \tag{10.8}$$

The 8 unknowns $\left(\varepsilon_i\,;K_i\right)$ (for each pixel) are estimated by a regularized ordinary least square method (Levenberg-Marquardt). Using the K_i (assuming the reflected part of the heat flux as constant in the temperature range 573K-673K), our experimental flux can be corrected to get rid of the reflection. Finally, the experimental flux is corrected for each pixel through the following relation:

$$n_{\lambda_i}^{\exp}\left(T_j\right) = M_{\lambda_i}^{\exp}\left(T_j\right) - K_i \qquad ,\forall i \in [\![1\,;4]\!] \;\; and \;\; \forall j \in [\![1\,;3]\!] \tag{10.9}$$

The aim is now to estimate using adjusted flux emitted by each pixel, the temperature field of the sample when the furnace is at T_2=*623K*. For this, we will find for each pixel the value of temperature *T* that minimizes the cost function (10.2).

Figures 7-10 show the averaged (1000 Images) thermographic images recorded by the camera through the four monochromatic filters $\lambda_{exp} = \{2\,;2.35\,;2.85\,;4\}\mu m$. The inscription "FT25" is indistinguishable at 2µm due to the low flux emitted but appears more and more clearly up to 4µm. The result of the temperature estimation by inversion of Planck's law (assuming unit emissivity) is given in Figure 11 for 4µm wavelength. As expected, we note that this simple estimation assuming a uniform emissivity does not correct the emissivity field because the pattern "FT25" is still visible on the calculated temperature field. Moreover, the estimation uncertainty of temperature is large (experimental temperature is about 623K), while the estimated temperature is about 587K (approximately 6% uncertainty or 40K) with a standard deviation of about 1.5K. Finally, Figure 12 shows the result of the estimated temperature (of about 625K) field given by the *TNL.Tabc* model (minimization of the cost function (10.2)). We note that the pattern has totally disappeared and that the temperature uncertainty is about 2K (0.3%) with a standard deviation of 4K. We have tried different models but the best results are given by the model *TNL.Tabc*, which allows us to take into account the emissivity variation over the wavelength range [2µm-4µm].

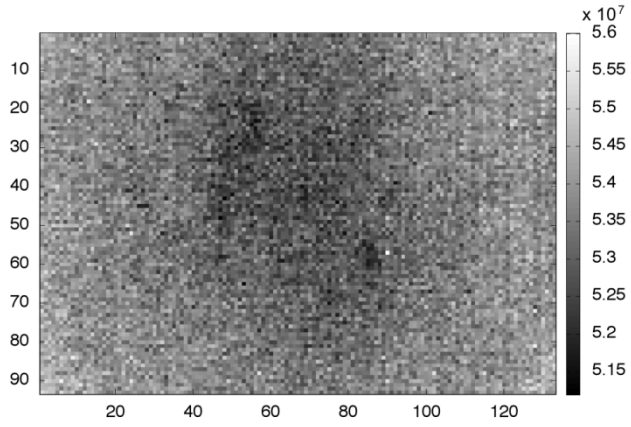

Figure 7. Flux 2µm.

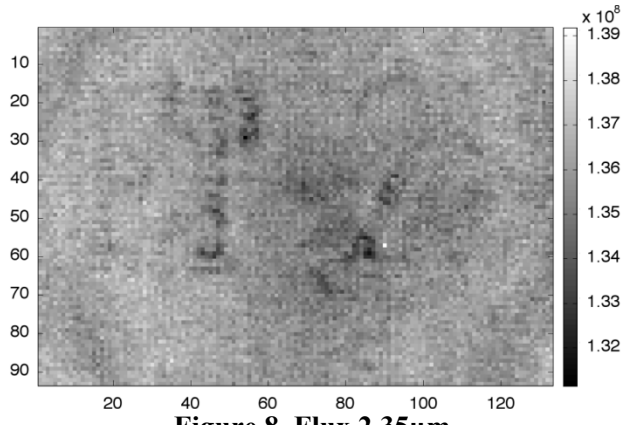

Figure 8. Flux 2.35µm.

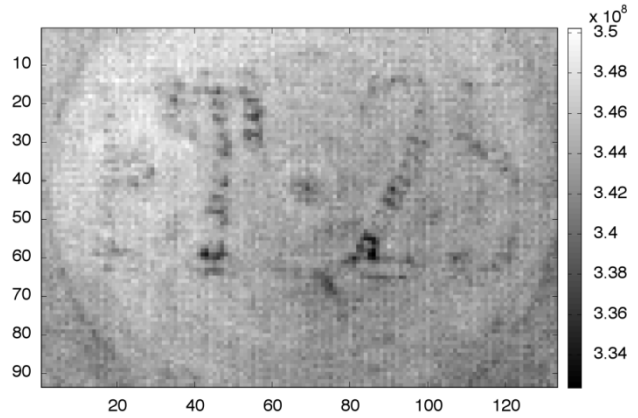

Figure 9. Flux 2.85µm.

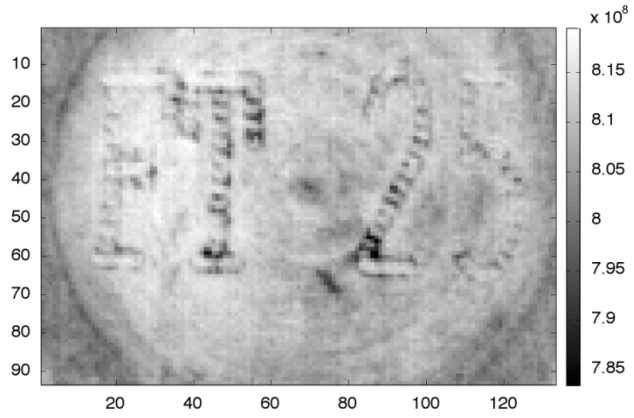

Figure 10. Flux 4µm.

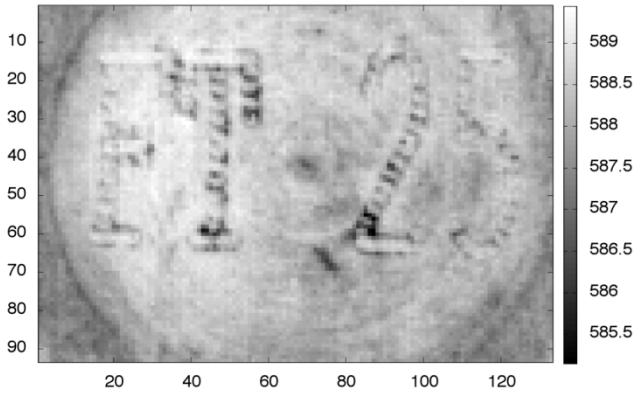

Figure 11. Estimated temperature: TCN 4µm.

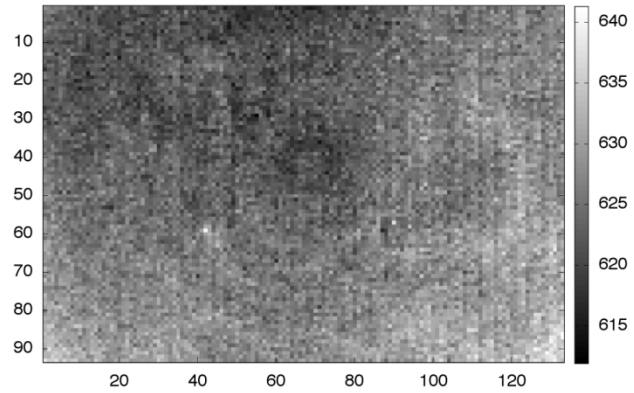

Figure 12. Estimated temperature: Tabc.

10.6 Conclusion

First, the results given by the unbiased model *TNL.Tabc* (10.1) (using fluxes without Wien's approximation and without fluxes ratio) and summarized in Table 2 are very satisfactory for emissivity variations of order between 0 and 2 (Drude model is a more difficult case). The inverse problem being numerically ill-conditioned, if the relative variation of the emissivity (or global spectral transfer function, including the emissivity) is known, it is preferable to use the lowest number of parameters allowing to model emissivity variations. However, in the absence of a priori knowledge about the emissivity, the *TNL.Tabc* model seems to be the best compromise.

Next, two different methods for selecting "optimal" wavelengths has been proposed: one through a sequential procedure and the other based on a global minimization with constraints which gives the best results. Although the iterative procedure is less efficient than the global minimization in term of temperature standard deviation, it presents the advantage to show the important of the choice of the different wavelengths.

To finish, the experimental results obtained using the *TNL.Tabc* model from the filters available experimentally $\boldsymbol{\lambda}_{exp} = \{2\ ;\ 2.35\ ;\ 2.85\ ;\ 4\}\,\mu m$ (close to theoretical optimal filters $\boldsymbol{\lambda}_{opt} = \{2.03\ ;\ 3.11\ ;\ 4.15\ ;\ 4.65\}\,\mu m$) are also very encouraging with an uncertainty of about 2K (0.3%) and a standard deviation of 4K.

10.7 References

[1] Souhar Y, Rémy B, Degiovanni A. Thermal Characterization of Anisotropic Materials at High Temperature through Integral Methods and Localized Pulsed Technique. International Journal of Thermophysics. 2013;34:322–340.

[2] Gardner JL, Jones TP, Davies MR. A six wavelength radiation pyrometer. High Temperatures – High Pressures. 1981;13:459-466.

[3] Meriaudeau F. Real time multispectral high temperature measurement: application to control in industry. Image and Vision Computing. 2007;25(7):1124–1133.

[4] Duvault T. Comparison between multiwavelength infrared and visible pyrometry: application to metals. Infrared Physics & Technology. 2008;51(4):292–299.

[5] Pierre T, Rémy B, Degiovanni A. Micro-scale temperature measurement by multi-spectral and statistic method in the ultraviolet-visible wavelengths. Journal of Applied Physics. 2008;103-1.

[6] Hervé P, Cedelle J, Negreanu I. Infrared technique for simultaneous determination of temperature and emissivity. Infrared Physics & Technology. 2012 Jan;55(1):1-10.

[7] Krapez J-C. Radiative measurements of temperature. In: Orlande HRB, Fudym O., Maillet D., Cotta RM, editors. Thermal measurements and inverse techniques. Boca Raton: CRC Press, Taylor & Francis Group, 2011, pp. 185-230.

Equation Chapter 11 Section 1